

Tuning of energy levels and optical properties of graphene quantum dots

Z. Z. Zhang and Kai Chang*

SKLSM, Institute of Semiconductors, Chinese Academy of Sciences, P. O. Box 912, Beijing 100083, China

F. M. Peeters

Departement Fysica, Universiteit Antwerpen, Groenenborgerlaan 171, B-2020 Antwerpen, Belgium

We investigate theoretically the magnetic levels and optical properties of zigzag- and armchair-edged hexagonal graphene quantum dots (GQDs) utilizing the tight-binding method. A new bound edge state at zero energy appears for the zigzag GQDs in the absence of a magnetic field. The magnetic levels of GQDs exhibit a Hofstadter-butterfly spectrum and approach the Landau levels of two-dimensional graphene as the magnetic field increases. The optical properties are tuned by the size, the type of the edge, and the external magnetic field.

PACS numbers: 73.22.-f, 78.67.-n, 75.75.+a, 81.07.Nb

Graphene is a single atomic layer consisting of a two-dimensional honeycomb lattice of carbon atoms. This novel system has attracted intense attention because of new fundamental physics and promising applications in nanoelectronics^{1,2}. It exhibits high crystal quality, an exotic Dirac-type spectrum, and ballistic transport properties on a submicron scale. Graphene samples are usually fabricated by micromechanical cleavage of graphite and have excellent mechanical properties that make it possible to sustain huge electric currents. The lateral confinement of Dirac fermions in graphene is still an enigmatic and extremely challenging task due to the well-known Klein paradox. The Klein paradox makes it impossible to localize the carriers in a confined region utilizing an electrostatic gate. The confinement of Dirac fermions at a nanometer scale is one of the central goals of graphene-based electronics and has attracted increasing interest^{3,4,5,6,7,8}. Recently it was demonstrated experimentally that graphene can be cut in the desired shape and size^{1,2}. Recent progresses in fabricating and characterizing stable graphene nanostructures provides the opportunity to explore the various remarkable optical^{9,10,11} and transport properties¹² of these structures.

In this work, we investigate theoretically the electronic structure and optical properties of zigzag- and armchair-edged hexagonal graphene quantum dots (GQDs) (see Fig. 1) utilizing the nearest-neighbor tight-binding model. The dangling bonds at the edges are passivated by hydrogen atoms. The model has been successfully used for fullerene molecules, carbon nanotubes, and other carbon-related materials^{13,14,15,16}. The Hamiltonian of GQDs can be written as $H = \sum_i \varepsilon_i c_i^\dagger c_i + \sum_{\langle i,j \rangle} t_{i,j} c_i^\dagger c_j$, where ε_i is the site energy, t_{ij} is the transfer energy between the nearest-neighbor sites, and c_i^\dagger (c_i) is the creation (annihilation) operator of the π electron at the site i . When considering a magnetic field B applied perpendicularly to the plane of a GQD, the transfer integral t_{ij} becomes $t_{ij} = t e^{i2\pi\phi_{i,j}}$, where $\phi_{ij} = \frac{e}{h} \int_{r_i}^{r_j} d\mathbf{l} \cdot \mathbf{A}$ is the Peierls phase. $\mathbf{A} = (0, Bx, 0)$ is the vector potential corresponding to the magnetic field B along the z

axis, which is perpendicular to the graphene plane. In our calculation, we take $\Phi_0 = h/e$ as the unit of the magnetic flux and $\Phi = \sqrt{3}Ba_0^2/2$ as the magnetic flux through a plaquette, where $a_0 = 2.46\text{\AA}$ is the lattice constant of graphite. The difference between the values of ε_i and t_{ij} for the atoms at the edge and the center is neglected. The relevant parameters used in our calculation are $\varepsilon = 0$, $t = -3.033$ ¹⁵. The eigenvalues and eigenstates can be obtained from the secular equation $\det|\varepsilon - H| = 0$, where $H_{ii} = 0$, $H_{\langle i,j \rangle} = t e^{i2\pi\phi_{i,j}}$.

Figs. 1 show electronic density distributions of the zigzag and armchair-edged graphene quantum dots (ZGQD and AGQD, respectively), in the absence of a magnetic field. The size of a dot is characterized by N , the number of hexagonal units along an edge. Figure 1(a) and 1(b) show the probability distributions of the highest valence level (HVL) and lowest conduction level (LCL) for the ZGQD with small size ($N = 2$). The probability distributions of the HVL and LCL correspond to the bonding and anti-bonding states that are localized at the corner of the hexagonal GQD. In contrast to conventional semiconductor quantum dots where the ground state is localized at the center of dot, the ground states for the conduction and valence bands, i.e., HVL and LCL, localize at the middle of each edge in the ZGQD (see Fig. 1(c) and (d)) as the size of the ZGQD increases. This feature can be understood as follows: the Dirac fermion in a ZGQD behaves like a confined photon in a cavity, and the lowest mode is the whispering gallery mode, which also localizes at the boundary of the cavity. The difference between the bonding and anti-bonding states becomes smaller as the size of the ZGQD increases. The difference between the edge states of a ZGQD and a graphene nanoribbon is that the edge state of the ZGQD localizes at the middle of the edge of GQD, in contrast to the homogeneously distributed edge state of a zigzag graphene nanoribbon^{14,17} or a zigzag triangular GQD¹⁸. This occurs because the contribution of each carbon atom at the edge of a ZGQD to the edge state is different, while it is the same for a zigzag nanoribbon or a zigzag triangular GQD. The density distributions of the LCL and HVL

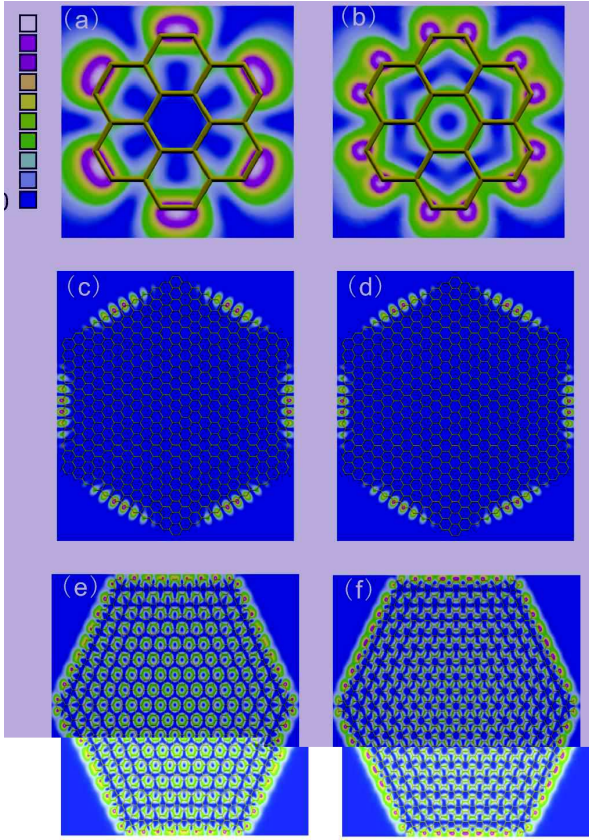


FIG. 1: (Color online) Electronic density distributions of the highest valence level (HVL) and lowest conduction level (LCL) in the absence of magnetic field. Panels (a) and (b): HVL and LCL for the $N_z = 2$ zigzag-edged graphene quantum dot (ZGQD). Panels (c) and (d): the same with $N_z = 12$. Panels (e) and (f): the same with armchair-edged graphene quantum dot (AGQD).

in an AGQD (see Figs. 1(e) and (f)) extend more completely over the whole GQD region and are very different from that in a ZGQD. This difference is indeed caused by the different topological geometry of the boundary of the graphene nanostructures.

Figs. 2(a) and (b) show the density of states (DOS) of ZGQDs and AGQDs, respectively, with different sizes in the absence of a magnetic field. The total number of the carbon atoms in ZGQD and AGQD are $6N_z^2$ and $6(3N_a^2 - 3N_a + 1)$, respectively. From the figures, we find that there is no edge state in a small ZGQD, and the edge state appears when the size of ZGQD increases according to the states at zero energy. Meanwhile, there is never an edge state for the AGQD. To demonstrate how the edge state appears, we plot the energy gap, i.e., the energy difference between the lowest conduction band level (LCL) and the highest valence band level (HVL), as a function of the size (N) of the GQD in Fig. 2(c). The energy gap decreases as the size of the GQD increases. Interestingly, the energy gap of the zigzag (armchair) GQD decays to zero quickly (slowly) as the size of the GQD increases.

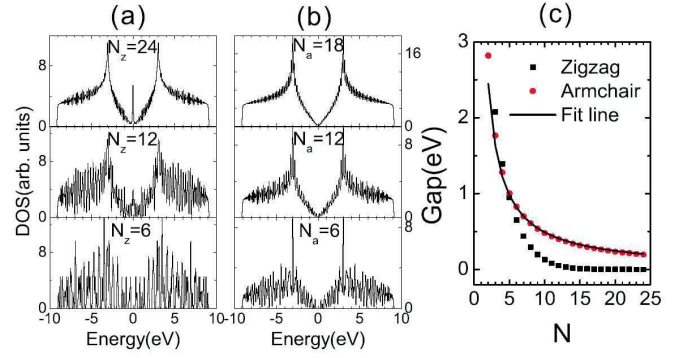


FIG. 2: (Color online) Density of states of ZGQD (a) and AGQD (b). We use a Gaussian function $f(E) = e^{-(E-E_0)^2/\Gamma^2}$ with a broadening factor $\Gamma = 0.05$ eV to smooth the discontinuous energy spectra. (c) The gap of ZGQD and AGQD as a function of the size, and the function of the fit line is a/N with $a = 4.9$ eV.

When the size of the AGQD approaches infinity, the gap decreases to zero, i.e., we recover the two-dimensional graphene case. The calculated energy gap for the AGQD falls off as $1/N \propto 1/L$ (see the solid line in Fig. 2(c)), where L is the length of each edge of the hexagonal GQD. This dependence of the band gap on the size of GQD is very different from that of a conventional semiconductor QD, which behaves as $1/L^2$.

Figs. 3(a) and 4(a) depict the magnetic field dependence of the energy spectrum of a ZGQD and AGQD exhibiting a clear Hofstadter butterfly characteristic, which is fractal and exhibits self-similarity^{14,20,21,22}. As the magnetic flux increases, the magnetic levels in the GQD, i.e., the so-called Fock-Darwin levels, approach the Landau levels (see the red lines in Figs. 3(b) and 4(b)) in graphene $E_n = \text{sgn}(n)(\sqrt{3}ta_0/2l_B)\sqrt{2|n|}$, where $l_B = \sqrt{\hbar/eB}$ is the cyclotron radius, n is an integer, and sgn is the sign function.

Figs. 3(c) and 4(c) show in detail how the magnetic levels of ZGQD and AGQD approach the zero-th Landau level at small magnetic flux. As magnetic flux increases, more energy levels approach the zero-th Landau level in pairs. The degeneracy of the energy level at zero energy will reach its maximum value $2N$ for $\Phi/\Phi_0 = 1/2N$. When the magnetic flux increases further, the degeneracy of the energy level at zero energy is lifted fast. This feature can also be seen in Fig. 3(d), which plots the DOS at the Dirac point. This figure indicates that the degeneracy, i.e., the number of energy levels at the zero energy, *approximately* decreases inverse linearly with the magnetic flux Φ/Φ_0 . These figures clearly demonstrate that the energy spectrum of the GQD possesses electron-hole symmetry when we neglect the second-nearest-neighbor interaction. The DOS and the magnetic level fan of the AGQD are similar to that of the ZGQD except at small magnetic flux. Comparing Fig. 3(c) to Fig. 4(c), the magnetic levels in the AGQD are distinct from those in the ZGQD at small magnetic flux, because the ZGQD

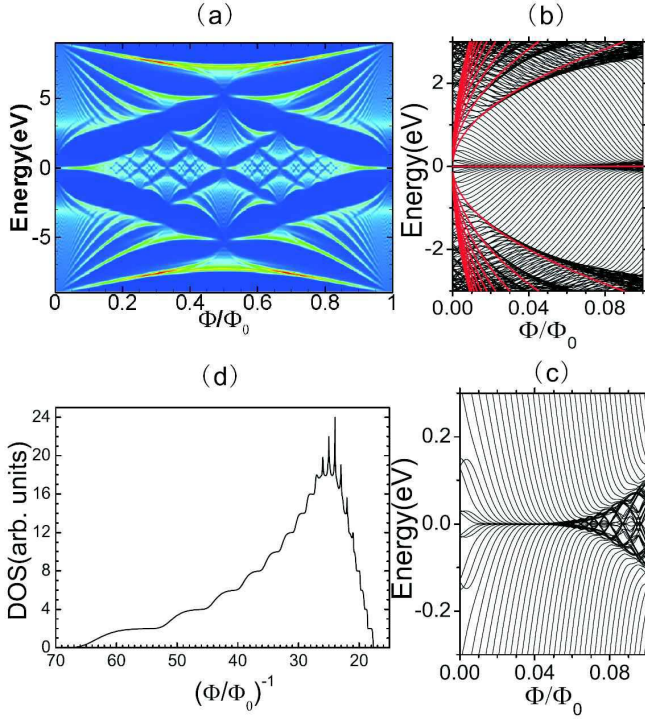


FIG. 3: (Color online) (a) The spectrum of the $N_z = 12$ ZGQD in a magnetic field. We use a Gauss function with a broadening factor of 0.1 eV to smooth discontinuous energy spectra. (b) and (c) the magnetic energy level fan near the Dirac point, i.e., the zero energy point. The red lines in (b) correspond to the Landau level of two-dimensional graphene. (d) the DOS at the Dirac point as a function of the inverse flux Φ/Φ_0 , where we use a Gauss function with a small broadening factor of 0.01 meV.

shows the edge state and AGQD does not for the levels near the Dirac point in absence of magnetic field. Therefore, the magnetic levels exhibit distinct behavior as the magnetic flux increases. The DOS of the AGQD (see Fig. 4(d)) also shows a step-like feature as the magnetic flux at the Dirac point increases.

Fig. 5 describes the density distributions of the LCL and HVL in the ZGQD and AGQD at small magnetic flux $\Phi/\Phi_0 = 0.01$. Interestingly, the density distributions of the LCL and HVL penetrate into the center of the GQD for the ZGQDs, which is very different from the AGQD case where both the electron and hole are dominantly localized in the center of the GQD. The density distributions for the ZGQD and AGQD show C_{6v} symmetry. This characteristic is caused by the magnetic confinement when the magnetic length l_B becomes comparable with the size of the GQD. In addition to those differences, the LCL and HVL of the zigzag GQD show opposite symmetry order with respect to that of the armchair GQD, i.e., the LCL (HVL) and HVL(LCL) of the ZGQD (AGQD) belong to the $E_1(E_2)$ and $E_2(E_1)$ representations at zero magnetic field (see Fig. 6).

The optical properties of GQDs are promising for

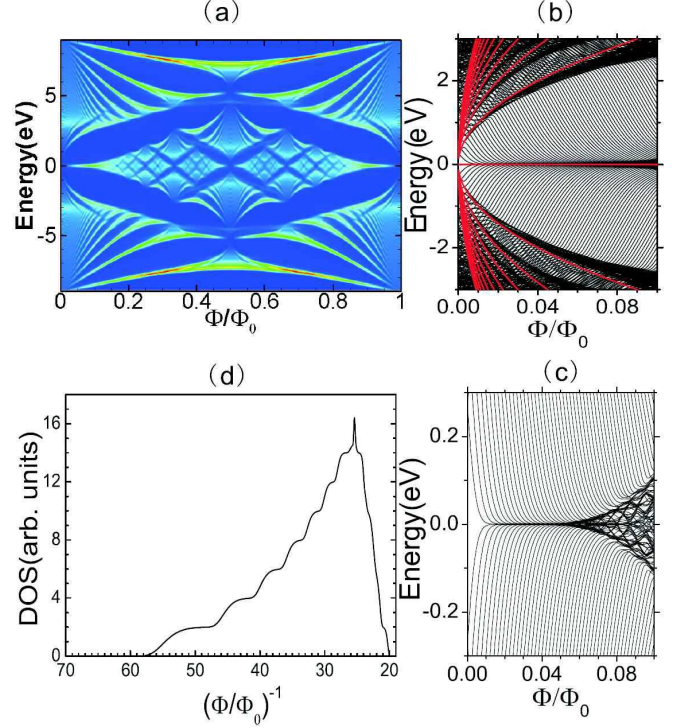


FIG. 4: (Color online) The same as Fig.3, but for the $N_a = 9$ AGQD

potential applications in optic-electronic devices based on graphene. Therefore, we calculate the absorption spectra of GQD $\alpha(\hbar\omega) = \frac{\pi e^2}{m_0^2 \epsilon_0 c n \omega V} \sum_{c,v} |\vec{\epsilon} \cdot \mathbf{P}_{cv}|^2 \times \delta(E_c - E_v - \hbar\omega)$, where n is the refractive index, c the speed of light in vacuum, ϵ_0 the permittivity of vacuum, m_0 the free-electron mass, and $\vec{\epsilon}$ is the polarization vector of the incident light along the x direction. The coupling between the sp_2 states and the p_z state is neglected since we are only interested in the optical properties of the GQD near the Dirac point, i.e., at the low energy regime. The momentum matrix¹⁹ is $\langle n | \mathbf{p} | m \rangle = im_0/\hbar \sum_{\mathbf{r}} \sum_{\mathbf{r}'} c_{\mathbf{r}}^* c_{\mathbf{r}'} (\mathbf{r}' - \mathbf{r}) \langle p_z, \mathbf{r} | H | p_z, \mathbf{r}' \rangle$.

The momentum operator $p_x(p_y)$ has E_2 symmetry and its direct product with all the irreducible representations of the C_{6v} group can be found in Table I. We divide the levels of the GQD into two different families: $A_1, A_3, E_1 \in \Omega_1$ and $A_2, A_4, E_2 \in \Omega_2$. The symmetry requires that only transitions between the valence band levels and the conduction band levels belonging to the different families Ω_1 and Ω_2 are allowed. Notice that the initial or final states of the transition should belong to the E_1 or E_2 representations. In Fig. 6(a) and (d), we label the level structure of a $N_z = 12$ and $N_a = 9$ GQD near the Dirac point as $C_1 - C_n$ for conduction bands with ascending order and $V_1 - V_n$ for valence bands with descending order, respectively. The conduction band levels C_i and valence band levels V_i belong to the distinct families Ω_1 and Ω_2 , respectively. For example, if C_i be-

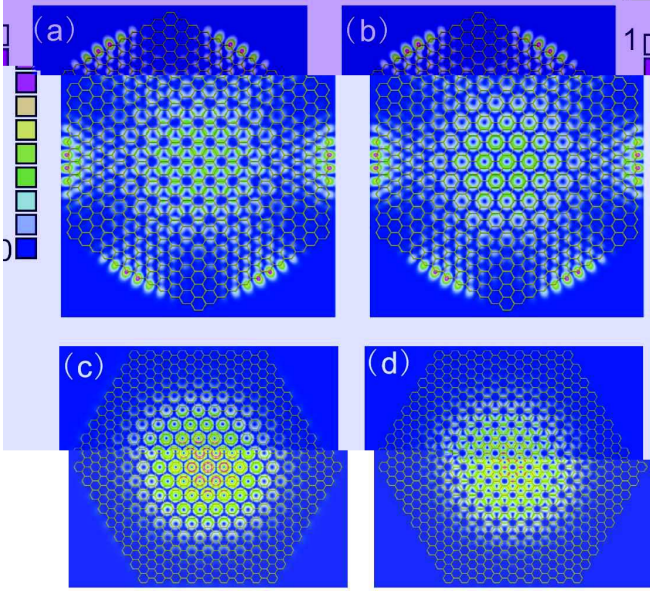


FIG. 5: (Color online) (a) and (b) show the density distributions of the HVL and LCL for the $N_z = 12$ ZGQD in the presence of the magnetic flux $\Phi/\Phi_0 = 0.01$, respectively. (c) and (d) the same as (a) and (b), but now for $N_a = 9$ AGQD.

TABLE I: Direct products of the E_2 representation for momentum operator $p_x(p_y)$ with all the irreducible representations of the C_{6v} group. The results are presented as direct sums of all possible irreducible representations of the C_{6v} group. The notations of symmetries are adopted from Ref. 23

Direct product	Direct sum
$E_2 \otimes A_1$	E_2
$E_2 \otimes A_2$	E_1
$E_2 \otimes A_3$	E_2
$E_2 \otimes A_4$	E_1
$E_2 \otimes E_1$	$A_2 \oplus A_4 \oplus E_2$
$E_2 \otimes E_2$	$A_1 \oplus A_3 \oplus E_1$

longs to the family Ω_1 , i.e., A_1, A_3 or E_1 , V_i must belong to the family Ω_2 , i.e., A_2, A_4 or E_2 , or *vice versa*. For zigzag GQDs with even N_z , the conduction band levels, from bottom to top, exhibit different symmetries, i.e., $E_2, A_3, E_1, A_2, \dots$, the corresponding valence band levels show $E_1, A_4, E_2, A_1, \dots$. For zigzag GQDs with odd N_z , the conduction band levels display the opposite (same) symmetries $E_1, A_4, E_2, A_1, \dots$ to the conduction (valence) band levels of zigzag GQDs with even N_z . For armchair GQDs, the lowest conduction band level always shows the symmetries $E_1, A_4, A_2, E_2, \dots$ from bottom to top and this order is independent of the size (N_a) of the armchair GQD.

For $N_z = 12$ ZGQD, the lowest optical-absorption peak (peak A) corresponds to the transition between the lowest conduction band level C_1 with E_2 symmetry

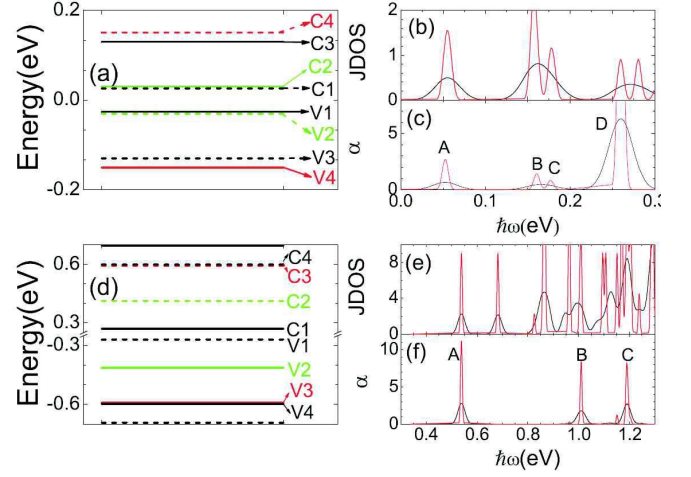


FIG. 6: (Color online) (a) and (d) are the level diagram for $N_z = 12$ ZGQD and $N_a = 9$ AGQD without the magnetic field, where different symmetries are represented by different colors and lines: black solid, black dashed, red solid, red dashed, green solid, and green dashed lines for the E_1, E_2, A_1, A_2, A_3 , and A_4 irreducible representations of the C_{6v} symmetry, respectively. (b) and (c) the JDOS and the optical absorption spectrum α for $N_z = 12$ ZGQD. We used a Gauss function with different broadening factors: 0.02 and 0.005 eV for the black and red line. (e) and (f) are the same as (b) and (c), but for $N_a = 9$ AGQD.

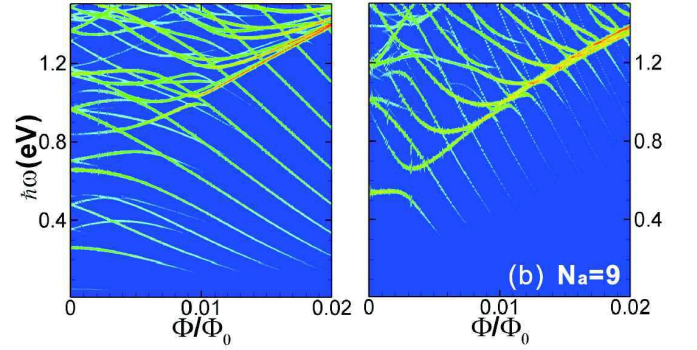


FIG. 7: (Color online) The contour plot of the magneto-optical spectra of zigzag (a) and armchair (b) GQD, respectively.

and the highest valence band level V_1 with E_1 symmetry. The second and third lowest transitions correspond to the transition between the level C_2 (C_3) with A_3 (E_1) symmetry and the level V_3 (V_2) with E_2 (A_4) symmetry and the level C_1 (C_4) and V_4 (V_1), respectively. But the strengths of these three transitions are very small, therefore these transitions are not clearly seen in the contour spectrum in Fig. 7 at $\Phi/\Phi_0 = 0$. The strong absorption peak (peak D) appears at $E = 0.26$ eV, corresponding to the transition between the level C_3 with E_1 symmetry and the level V_3 with E_2 symmetry. This strong absorption arises from the large moment matrix $\langle n | \mathbf{p} | m \rangle$ between these states.

For $N_a = 9$ AGQD, the lowest peak (peak A) is similar to that in the zigzag GQD, corresponding to the transition between C_1 and V_1 . But the second peak (peak B) is different from those of the zigzag GQD. This peak corresponds to the transition between the level C_2 (C_4) with A_4 (E_2) symmetry and the level V_4 (V_2) with E_1 (A_3) symmetry. The third strong peak (peak C) indicates the transition between the level C_4 with E_2 symmetry and the level V_4 with E_1 symmetry. Strong absorption takes place when the initial (V_i) and final states (C_i) have either E_1 symmetry or E_2 symmetry. As the size of the GQD increases, the absorption peaks shift to long wavelength for both ZGQD and AGQD. The absorption peaks of the ZGQD shift to the long wavelength faster than those of the AGQD. The relative strength between the peak D and A increases as the size of the GQD increases for ZGQDs. But for AGQDs, the relative strength between the peak C and A is almost independent of the size.

Next, we discuss the effect of a magnetic field on the optical spectrum of a GQD. Here, we only focus on the small magnetic flux case (see Fig. 7). The spectra of two distinct GQDs, zigzag and armchair GQD, exhibit quite different behavior due to their different level structures and the oscillator strengths determined by the boundary, especially for the LCL and HVL which localize at the edge of ZGQD. The spectra of two distinct GQDs show that the strengths of the transitions vary as the magnetic field increases. In particular, the strong absorption

lines exhibit \sqrt{B} asymptotic behavior corresponding to the transitions between the conduction and valence band Landau levels at high magnetic field. We also find anti-crossings in the spectra, since the magnetic field induces the mixing of the levels belonging to the different families.

In summary, we investigated theoretically the magnetic levels and the optical spectrum in GQDs. In contrast to conventional semiconductor QDs, the LCL and HVL exhibit an edge-state feature, i.e., a non-zero probability of being at the edge of the sample, and the density distribution depends sensitively on the type of boundary of GQDs and the magnetic field strength. The magnetic levels of GQD display a Hofstadter butterfly characteristic, and approach the Landau levels of two-dimensional graphene as the magnetic field increases. The magneto-optical spectrum of a graphene quantum dot in the interesting energy range (0-3 eV) is promising for carbon-based electronics applications. The position and strength of the absorption peaks can be tuned by the size of the GQD, the type of the edge of the GQD, and the external magnetic field.

Acknowledgments

This work is supported by the NSF of China Grant No. 60525405 and the Flander-China bilateral programme.

* Corresponding author: kchang@red.semi.ac.cn

- ¹ K. S. Novoselov, A. K. Geim, S. V. Morozov, D. Jiang, Y. Zhang, S. V. Dubonos, I. V. Grigorieva and A. A. Firsov, *Science* **306**, 666 (2004); H. Hiura, *Appl. Surf. Sci.* **222**, 374 (2004); Y. Zhang, J. W. Tan, H. L. Stormer and P. Kim, *Nature (London)* **438**, 201 (2005); A. K. Geim, and K. S. Novoselov, *Nature Materials* **6**, 183 (2007).
- ² K. S. Novoselov, *Nature (London)* **438**, 197 (2005).
- ³ P. G. Silvestrov and K. B. Efetov, *Phys. Rev. Lett.* **98**, 016802 (2007).
- ⁴ A. DeMartino, L. Dell'Anna, and R. Egger, *Phys. Rev. Lett.* **98**, 066802 (2007).
- ⁵ H. Y. Chen, V. Apalkov, and T. Chakraborty, *Phys. Rev. Lett.* **98**, 186803 (2007).
- ⁶ J. M. Pereira, Jr., P. Vasilopoulos, and F. M. Peeters, *Nano. Lett.* **7**, 946 (2007).
- ⁷ B. Trauzettel, D. V. Bulaev, D. Loss, and G. Burkard, *Nature Phys.* **3**, 192 (2007).
- ⁸ T. G. Pedersen, C. Flindt, J. Pedersen, N. A. Mortensen, A.-P. Jauho, and K. Pedersen, *Phys. Rev. Lett.* **100**, 136804 (2008).
- ⁹ M. O. Goerbig, J. N. Fuchs, K. Kechedzhi, and V. I. Fal'ko, *Phys. Rev. Lett.* **99**, 087402 (2007).
- ¹⁰ V. P. Gusynin, S. G. Sharapov, and J. P. Carbotte, *Phys. Rev. Lett.* **98**, 157402 (2007).
- ¹¹ H. Hsu and L. E. Reichl, *Phys. Rev. B* **76**, 045418 (2007).
- ¹² B. Ozyilmaz, P. Jarillo-Herrero, D. Efetov, D. A. Abanin,

- L. S. Levitov, and P. Kim, *Phys. Rev. Lett.* **99**, 166804 (2007).
- ¹³ K. Nakada, M. Fujita, G. Dresselhaus, and M. S. Dresselhaus, *Phys. Rev. B* **54**, 17954 (1996).
- ¹⁴ K. Wakabayashi, M. Fujita, H. Ajiki, and M. Sigrist, *Phys. Rev. B* **59**, 8271 (1999).
- ¹⁵ R. Saito, G. Dresselhaus, and M. S. Dresselhaus, *Physical Properties of Carbon Nanotubes* (Imperial College Press, London, 1998).
- ¹⁶ M. Ezawa, *Phys. Rev. B* **73**, 045432 (2006).
- ¹⁷ L. Brey and H. A. Fertig, *Phys. Rev. B* **73**, 235411 (2006).
- ¹⁸ T. Yamamoto, T. Noguchi, and K. Watanabe, *Phys. Rev. B* **74**, 121409(R) (2006).
- ¹⁹ T. G. Pedersen, K. Pedersen, and T. B. Kriestensen, *Phys. Rev. B* **63**, 201101(R) (2001).
- ²⁰ D. R. Hofstadter, *Phys. Rev. B* **14**, 2239 (1976); R. Rammal, *J. Phys. (Paris)* **46**, 1345 (1985).
- ²¹ Y. Hatsugai, T. Fukui, and H. Aoki, *Phys. Rev. B* **74**, 205414 (2006).
- ²² N. Nemec and G. Cuniberti, *Phys. Rev. B* **75**, 201404 (2007).
- ²³ G. L. Bir and G. E. Pikus, *Symmetry and Strain Induced Effects in Semiconductors* (Wiley, New York, 1974); G. F. Koster, J. O. Dimmock, R. G. Wheeler, and H. Slatz, *Properties of the Thirty-Two Point Groups* (MIT Press, Cambridge, 1966).